Blister Formation in Ion-Implanted GaAs: Role of Diffusivity

R. R. Collino,[1] B. B. Dick,[2] F. Naab,[2] M. D. Thouless,[1,3] and R. S. Goldman[3]*

[(1)] *Department of Mechanical Engineering, University of Michigan,*

[(2)] *Department of Nuclear Engineering and Radiological Sciences, University of Michigan,*

[(3)] *Department of Materials Science and Engineering, University of Michigan,*

Ann Arbor, MI 48109-2136

Y. Q. Wang

Los Alamos National Laboratory, Los Alamos, NM 87545

We have investigated the influence of substrate temperature during implantation, T_{implant}, on blister formation in GaAs:N layers produced by N ion implantation followed by rapid thermal annealing. Similar depths of popped blisters (craters) and damage profiles were observed for both low and high T_{implant}. This is in contrast to reports of T_{implant}-dependent blister formation in higher-diffusivity systems such as GaAs:H and Si:H. The apparent T_{implant}-insensitivity of blister formation in GaAs:N is likely due to the lower diffusivity of N in GaAs in comparison to that of H in GaAs and Si.

Localized surface deformation caused by the internal gas pressure of sub-surface flaws or by residual stresses within near-surface layers is often termed "surface blistering," and has been observed following processes which involve ion-solid interactions.[1] These processes range from H^+ and D^+ irradiation-induced erosion of reactors to layer transfer by ion-cut following H^+ implantation into semiconductors.[2] Implantation-induced gas bubbles have been revealed by transmission electron micrographs of voids[3] and by gas emission associated with bursting of surface blisters.[4] In semiconductors, studies of implantation-induced blistering have focused on light ions (H or He) in Si and GaAs. In Si:H, bubble and blister formation has been attributed to diffusion of implanted ions into extended lattice defects (platelets).[3] In GaAs:H, blister formation has been reported within a T_{implant} window ranging from ~120 to ~300 °C.[5,6] Interestingly, in GaAs:H, the extent and depth-dependence of lattice disorder increases with T_{implant},[5,6] up to ~300 °C. Above ~300 °C, out-diffusion of hydrogen prevents the accumulation of gas required for bubble formation.[5] For several semiconductors implanted with light ions, bubble and blister formation are also dependent on the T_{implant}, and occur only within a temperature window that is specific to the particular ion-matrix system.[7,8] For the systems studied to date, it has been suggested that the lower-temperature bound is determined by lattice damage, while the upper-temperature bound is limited by the ion-matrix diffusivity.[7] In this work, we demonstrate the key role of diffusion on the T_{implant}-dependence of blister formation. We focus on GaAs:N, which exhibits low diffusivity for both highly-damaged[9] and crystalline[10] systems. For GaAs:N layers produced by N-implantation into GaAs followed by rapid-thermal annealing (RTA), we report a T_{implant}-insensitivity of crater (popped blister) depths and damage depth profiles, due to the insignificant ion-matrix diffusivity in this case.

For this study, ~1 µm thick GaAs films (undoped or Si-doped) were grown by molecular-beam epitaxy on (001) GaAs. To induce both nanocrystal formation and blistering, these high purity films were implanted with 100 keV N^+ at a fluence of 5 x 10^{17} cm^{-2}, as described in earlier reports.[11,12] To minimize ion channeling, a ~7° ion beam angle of incidence with respect to the sample surface normal was utilized. During implantation, the substrate temperature was maintained at -196 °C or 300 °C; we will refer to the corresponding samples as "low-*T* implanted" and "high-*T* implanted," respectively. RTA was performed in N_2 gas for 30 sec at 800 °C, as discussed in Ref. 12. Tapping-mode atomic force microscopy (AFM) was performed in a Digital Instruments NanoScope IIIA, using etched Si tips. The retained N dose and the depth-dependence of the N concentration, [N], were determined with nuclear reaction analysis (NRA) using the $^{14}N(d,\alpha_1)^{12}C$ reaction,[13] as described in Ref. 14. The depth-dependence of lattice disorder was determined by channeling-Rutherford backscattering spectrometry (RBS) with a 2 MeV He^{++} beam, in conjunction with SIMNRA simulations.

To examine the origins of blister formation, we compared scanning electron micrographs (SEM) of the surfaces of (a) as-grown, (b) as-grown-plus-annealed, (c) high-*T*-implanted, and (d) high-*T*-implanted-plus-annealed GaAs layers. As shown in Figs. 1(a) and 1(c), the surfaces of the as-grown and as-implanted layers appear featureless. The surface features apparent on the annealed GaAs surface, shown in Fig. 1(b), are likely due to As loss during RTA.[11] Surface blisters and craters (popped blisters) are observed in the implanted-plus-annealed case shown in Fig. 1(d). Thus, it appears that blister formation results from subsurface N_2 gas accumulation during RTA.

The normalized NRA yields vs. ion energy for low- and high-*T*-implanted layers are shown in Fig. 2. The similar ion-energy-dependence of the yields suggests similar N depth

profiles in both cases. The retained fluence of low- and high-*T*-implanted layers, estimated from integrals of the peak areas, are (4.9±0.3) and (4.8±0.3) x 10^{17} cm^{-2}. The similarity of these values to that of the target dose ($5.0x10^{17}$ cm^{-2}) indicates near-complete N retention in GaAs:N, even at 300 °C. This is in contrast to GaAs:H, for which retained H fluence in a 300 °C implant was 32% lower than that for a -90 °C implant,[5] presumably due to H out-diffusion.

Post-annealing surface morphology and local variations in crater depths were examined using SEM and AFM images of low-*T* (high-*T*) implanted-plus-annealed layers, as shown in Figs. 3(a) (3(c)) and 3(b) (3(d)). In both cases, SEM images reveal blistered surfaces with similar feature sizes and densities. Examples of ~2 μm diameter blisters and craters are highlighted in Fig. 3(a) and 3(c) by solid and dashed circles, respectively. Line-cuts from the AFM images in Figs. 3(b) and 3(d) reveal ~200 nm crater depths for both the low- and high-*T* implanted-plus-annealed layers. The similarity of these crater depths with the depth of the maximum [N] predicted by SRIM simulations, as well as the nearly complete retention of implanted N discussed above, suggest insignificant diffusion of N during the annealing step.

To compare damage depth distributions, (001) channeling-RBS measurements were performed in implanted layers. Figure 4 presents the normalized yield vs. energy and depth for low-*T* and high-*T* (a) implanted and (b) implanted-plus-annealed GaAs layers. For comparison, random and (001) channeling yields from GaAs are included on the plots. The ratio of the channeling-RBS yield to the random case, χ, is a measure of the fraction of ions which were de-channeled, presumably due to lattice disorder. For both the low-*T* and high-*T*-implanted layers, similar depth-dependencies of the normalized yield are apparent in Fig. 4(a), suggesting similar damage depth profiles for both cases. The low-*T*-implanted sample exhibits a slightly wider depth profile (at ~300 nm) compared to that of the high-*T*-implanted sample. Although the

minor differences between the spectra are at the level of the detector energy resolution (±20 keV), similar shifts in damage recovery with increasing $T_{implant}$ have been reported in GaAs:N.[15] Yet, this similarity in GaAs:N is in contrast to the significant $T_{implant}$-dependence of both normalized yield and depth profile of backscattered ions observed in -90 to 320 °C-implanted GaAs:H.[5,6]

The energy-dependence of the normalized RBS yield for implanted layers following annealing is presented in Fig. 4(b). The annealed layers (without implanted N) exhibit a near-surface maximum at ~1580 keV, most likely due to As loss from the top ~50 nm of the layer. In addition, the implanted-plus-annealed layers exhibit a local maximum in the normalized RBS yield at ~1480 keV, which corresponds to a depth of ~200 nm beneath the surface. The value of this local maximum in yield is similar to that of the random GaAs case, and its depth corresponds to that of the observed bubble formation,[12] as well as to the predicted depth of maximum [N] and crater depth formation shown in Fig. 2. Thus, it is likely that this local maximum in yield is due to de-channeling of He^{++} at the Ga or As atoms displaced by N bubble-induced internal surfaces and strain fields, confirming the *T*-insensitivity of bubble formation depths.

The $T_{implant}$-insensitivity of crater depths, average damage depth profiles, and ion depth profiles for GaAs:N can be explained in the context of diffusivity-driven blister formation. In GaAs, $T_{implant}$-dependent blistering has been observed for implantation of H[5,6] and/or He[16] ions, both of which exhibit substantially higher diffusivities than that of N in GaAs at the implantation temperature ranges associated with blister formation.[17] For example, the absence of surface blistering on GaAs:H for $T_{implant} > 300$ °C[5] is likely related to the significant H re-distribution and out-diffusion reported for $T_{implant} > 200$ °C.[19] Similarly, in Si:H, an upper-bound $T_{implant}$ for blister formation of ~450 °C is reported,[7] and for high dose, room temperature-implanted Si:H,[20]

blister formation was not observed, presumably due to enhanced H diffusivity in that case.[21] Indeed, H diffusion in both Si[21] and GaAs[18] has been reported to depend on lattice damage, presumably due to the dominance of a vacancy-assisted interstitial diffusion process. In contrast, the observed damage-insensitivity of blister formation in GaAs:N is likely related to an interstitial kick-out diffusion mechanism which would not be influenced by vacancies.[10]

The role of diffusivity in bubble formation is further supported by comparison of exfoliation in GaAs:N and Si:H. In Si:H, with increasing T_{implant}, the exfoliation depth varies from the depth of maximum ion concentration to that of maximum lattice damage,[22] where presumably a higher concentration of extended defects act as bubble nucleation sites. On the other hand, in GaAs:N, the exfoliation depth remains at the depth of maximum ion concentration, even for high-T implantation and annealing. Thus, in the case of a low-diffusivity system, diffusion is inhibited and the exfoliation depth is likely to be controlled by the projected ion range. These results suggest that ion-matrix diffusivity influences the temperature-dependence of blister formation.

In summary, we have examined the influence of T_{implant} on blister formation in GaAs:N. Local crater depths, average damage depth profiles, and retained N doses were similar for both low-T and high-T implantations. This is in contrast to the T_{implant}-dependence of these parameters observed in light ion, high-diffusivity systems such as GaAs:H and Si:H. Thus, the low diffusivity of N in GaAs, which is independent of the extent of lattice damage, leads to T_{implant}-insensitive exfoliation depths and damage depth profiles. Therefore, low ion-matrix diffusivity may be beneficial for the stable precipitation of bubbles across a wide range of processing temperatures.

This work was supported by NSF through Grant No. CMMI-0700301 monitored by Clark Cooper. RC was supported in part by an NSF Graduate Research Fellowship and the Michigan Memorial Phoenix Energy Institute. We gratefully acknowledge the support of the Center for Integrated Nanotechnologies at Los Alamos National Laboratory as well as the assistance of the staff at the Michigan Ion Beam and Electron Microscopy and Analysis laboratories at UM. The ion implanter at MIBL is supported by NSF Grant No. DMR-0520701.

References

1. B. M. U. Scherzer, in *Topics in Applied Physics: Sputtering by particle bombardment II*, edited by R. Behrisch (Springer, Berlin, 1983), Vol. **52**, Chap. 7, p. 271-355.

2. M. Bruel, Electron. Lett. **31**, 1201 (1995).

3. M. K. Weldon, V. E. Marisco, Y. J. Chabal, A. Agarwal, D. J. Eaglesham, J. Sapjeta, W. L. Brown, D. C. Jacobson, Y. Caudano, S. B. Christman, and E. E. Chaban, J. Vac. Sci. Technol. B **15,** 1065 (1997).

4. B. Terreault, G. Ross, R. G. St.-Jacques, and G. Veilleux, J. Appl. Phys. **51**, 1491 (1980).

5. M. Webb, C. Jeynes, R. Gwilliam, P. Too, A. Kozanecki, J. Domagala, A. Royle, and B. Sealy, Nucl. Instrum. Methods Phys. Res. B **240**, 142 (2005).

6. G. Gawlik, R. Ratajczak, A. Turos, J. Jagielski, S. Bedell, and W. L. Lanford, Vacuum **63**, 697 (2001).

7. Q.-Y. Tong, L.-J. Huang, and U. M. Gösele, J. Electron. Mater. **29**, 928 (2000).

8. P. Chen, Z. Di, M. Nastasi, E. Bruno, M. G. Grimaldi, N. D. Theodore, and S. S. Lau, Appl. Phys. Lett. **92**, 202107 (2008).

9. S. Amine, G. Ben Assayag, C. Bonafos, B. de Mauduit, H. Hidriss, and A. Claverie, Mater. Sci. Eng., B **93**, 10 (2002).

10. G. Bösker, N. A. Stolwijk, J. V. Thordson, U. Södervall, and T. G. Andersson, Phys. Rev. Lett. **81**, 3443 (1998).

11. X. Weng, W. Ye, S. J. Clarke, R. S. Goldman, V. Rotberg, A. Daniel, and R. Clarke, J. Appl. Phys. **97**, 064301 (2005).

12. X. Weng, W. Ye, R. S. Goldman, and J. C. Mabon, J. Vac. Sci. Technol. B **22**, 989 (2004).

13. S. Pellegrino, L. Beck, and P. Trouslard, Nucl. Instrum. Methods Phys. Res. B **219-220**, 140 (2004).

14. M. Reason, H. A. McKay, W. Ye, S. Hanson, R. S. Goldman, and V. Rotberg, Appl. Phys. Lett. **85**, 1692 (2004).

15. A. Turos, A. Stonert, B. Breeger, E. Wendler, W. Wesch, and R. Fromknecht, Nucl. Instrum. Methods Phys. Res. B **148**, 401 (1999).

16. I. Radu, PhD Thesis, Max Planck Institute of Microstructure Physics, Halle, Germany, 2003.

17. Based on diffusivity, *D*, data for GaAs:N at ~800 °C (Ref. 9), D(300 °C) ~ 10^{-17} cm^2s^{-1}. For GaAs:H, D(300 °C) ~10^{-14} cm^2s^{-1} (Ref. 18). For GaAs:He, D(300 °C) ~ 10^{-13} cm^2s^{-1} (Ref. 16).

18. J. Räisänen, J. Keinonen, V. Karttunen, and I. Koponen, J. Appl. Phys. **64**, 2334 (1988).

19. J. M. Zavada and R. G. Wilson, Mat. Sci. Forum **148-149**, 189 (1994).

20. V. P. Popov, I. E. Tyschenko, L. N. Safronov, O. V. Naumova, I. V. Antonova, A. K. Gutakovsky, and A. B. Talochkin, Thin Solid Films **403-404**, 500 (2002).

21. B. L. Sopori, X. Deng, J. P. Benner, A. Rohatgi, P. Sana, S. K. Estreicher, Y. K. Park, and M. A. Roberson, Sol. Energy Mater. Sol. Cells **41-42**, 159 (1996).

22. J. K. Lee, M. Nastasi, N. D. Theodore, A. Smalley, T. L. Alford, J. W. Mayer, M. Cai, and S. S. Lau, J. Appl. Phys. **96**, 280 (2004).

FIGURES

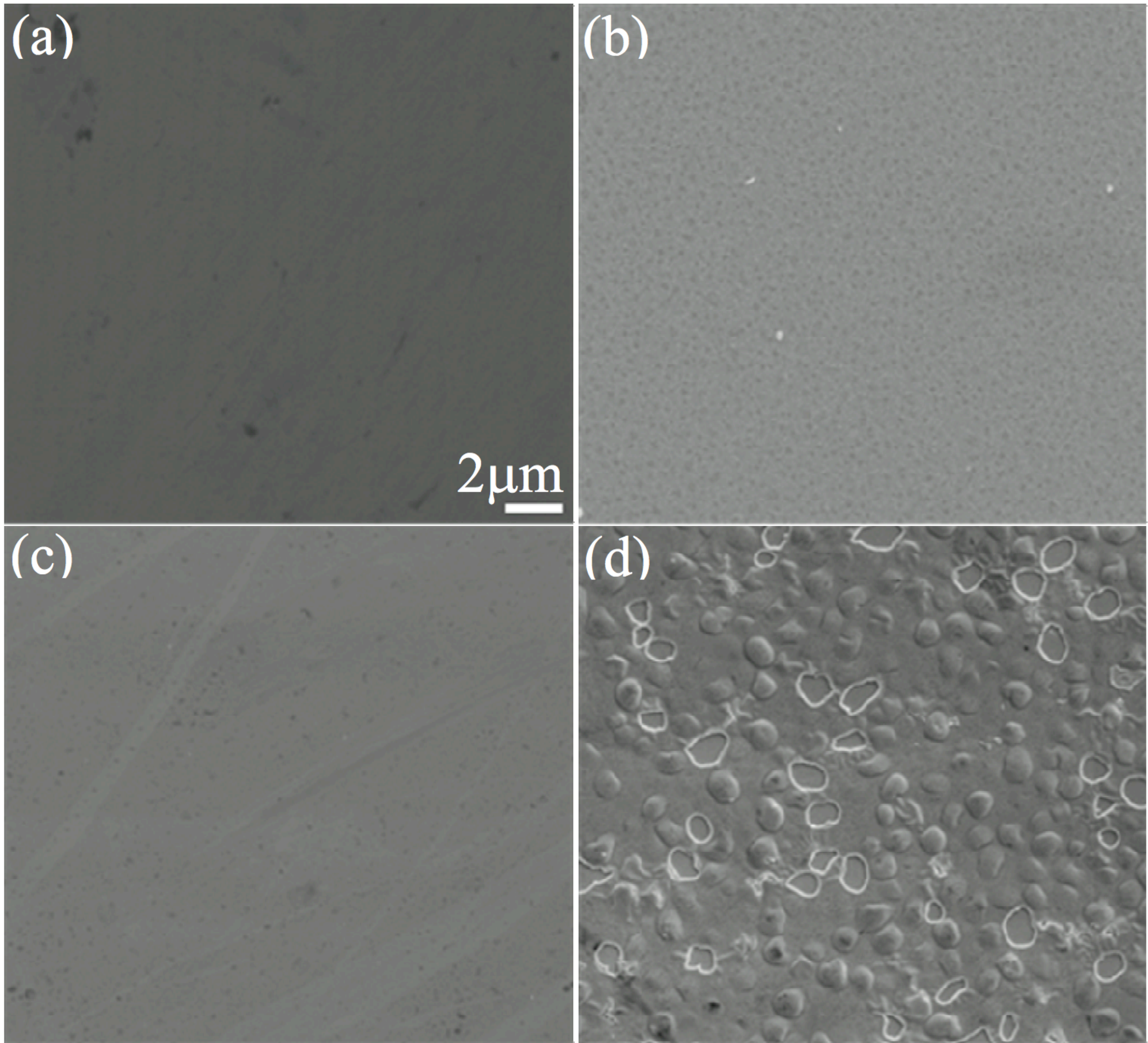

Fig. 1: SEM images of (a) as-grown (b) annealed (c) high-*T*-implanted and (d) high-*T*-implanted-plus-annealed GaAs. Surface features are not apparent in both (a) as-grown and (c) high-*T*-implanted samples. For the (b) annealed and (d) high-*T*-implanted-plus-annealed films, surface pitting and blistering are apparent, respectively.

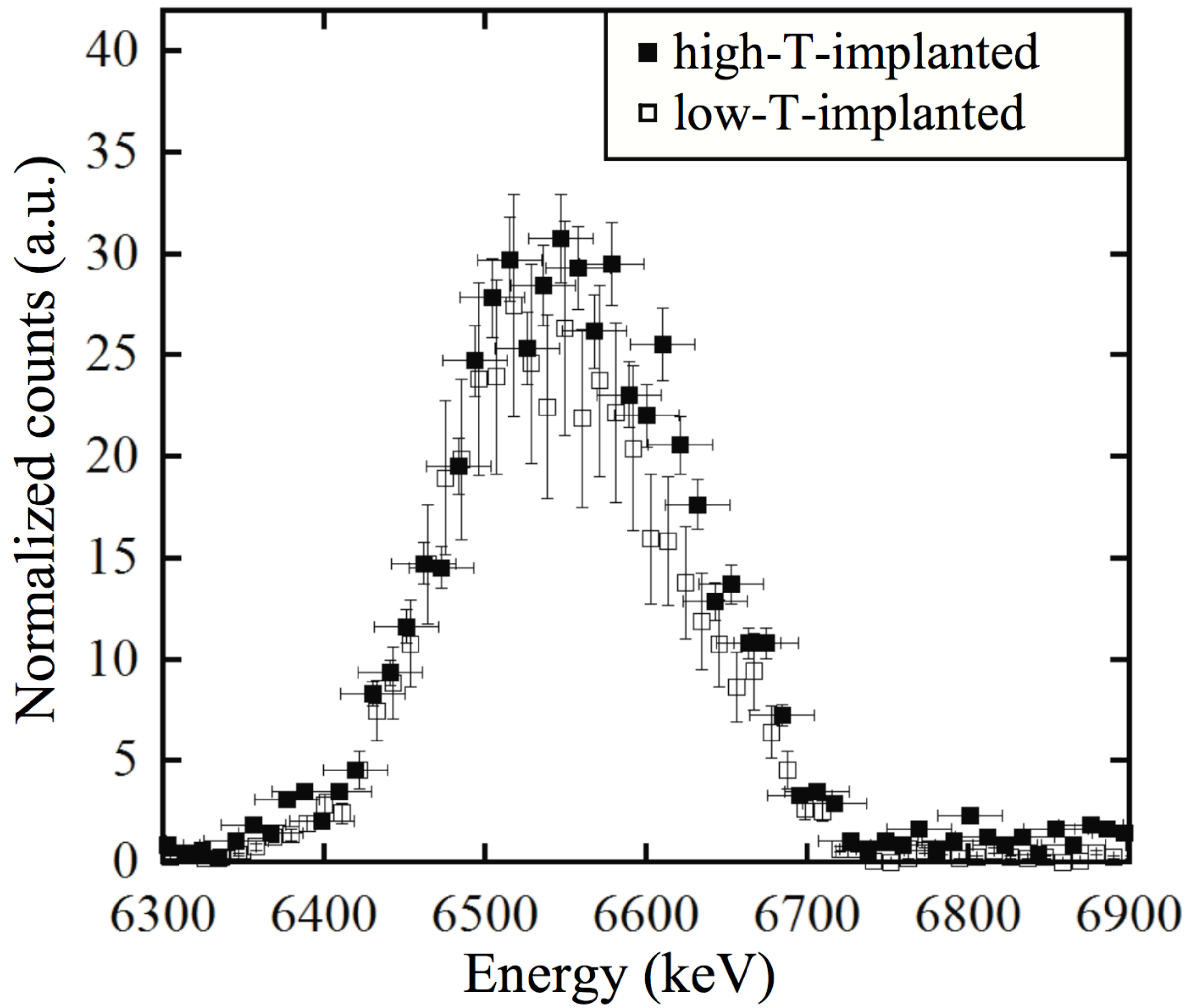

Fig. 2: NRA spectra of α_1 particle yield vs. energy in low-*T* and high-*T*-implanted GaAs. The similarity of counts vs. energy between the two samples indicates that the retained fluence (estimated from integrated peak areas) and [N] depth profile are similar for both.

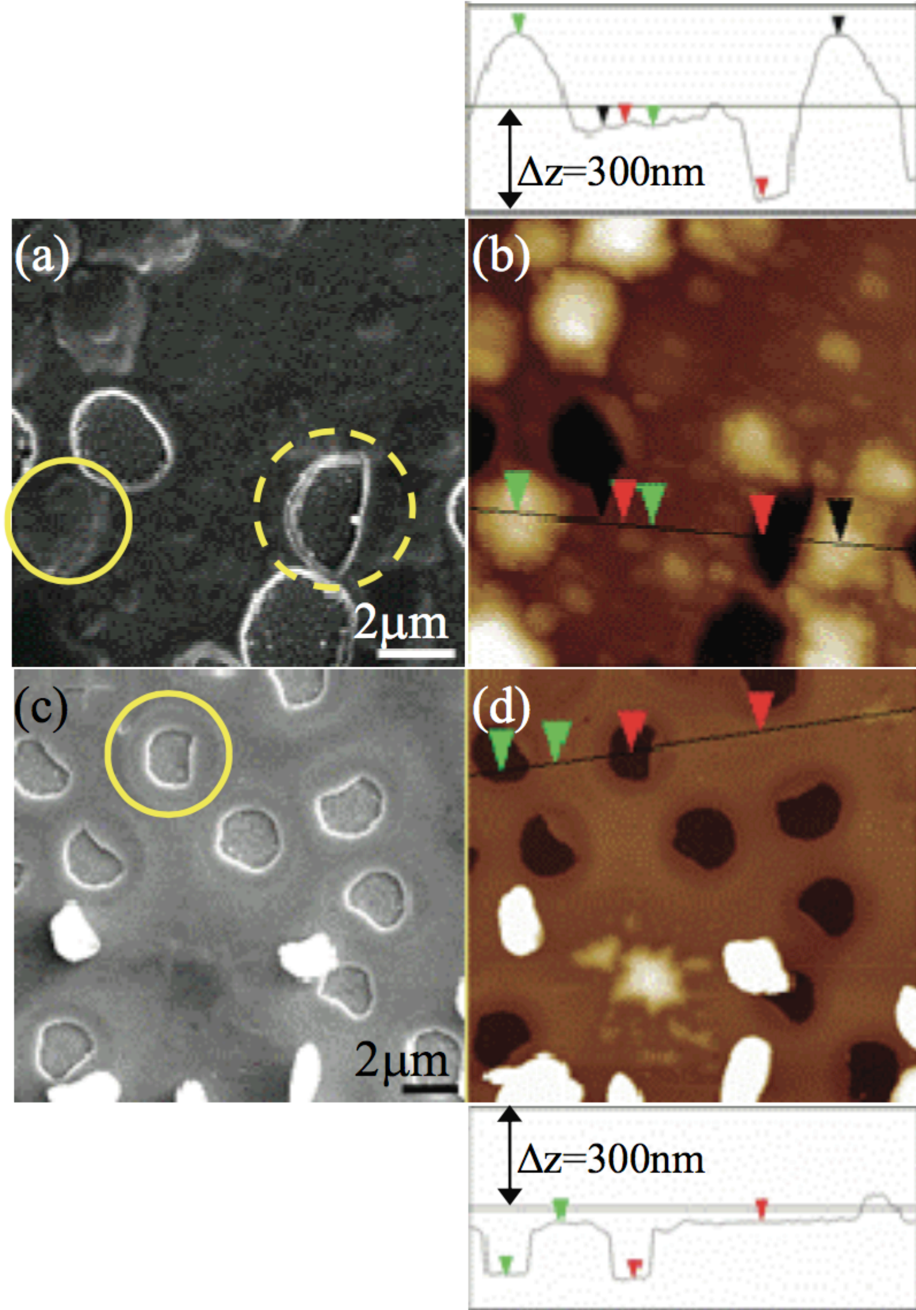

Fig. 3: (Color online) SEM (AFM) images of (a, (b)) low-*T*-implanted and (c, (d)) high-*T*-implanted-plus-annealed samples. SEM images in (a) and (c) reveal circular blisters and craters ~2 μm in diameter (highlighted with solid and dashed circles, respectively in (a)) for both low- and high-temperature implantations. AFM images of the same areas are shown in (b) and (d). The cross-sectional profiles reveal crater depths of ~200 nm in both cases.

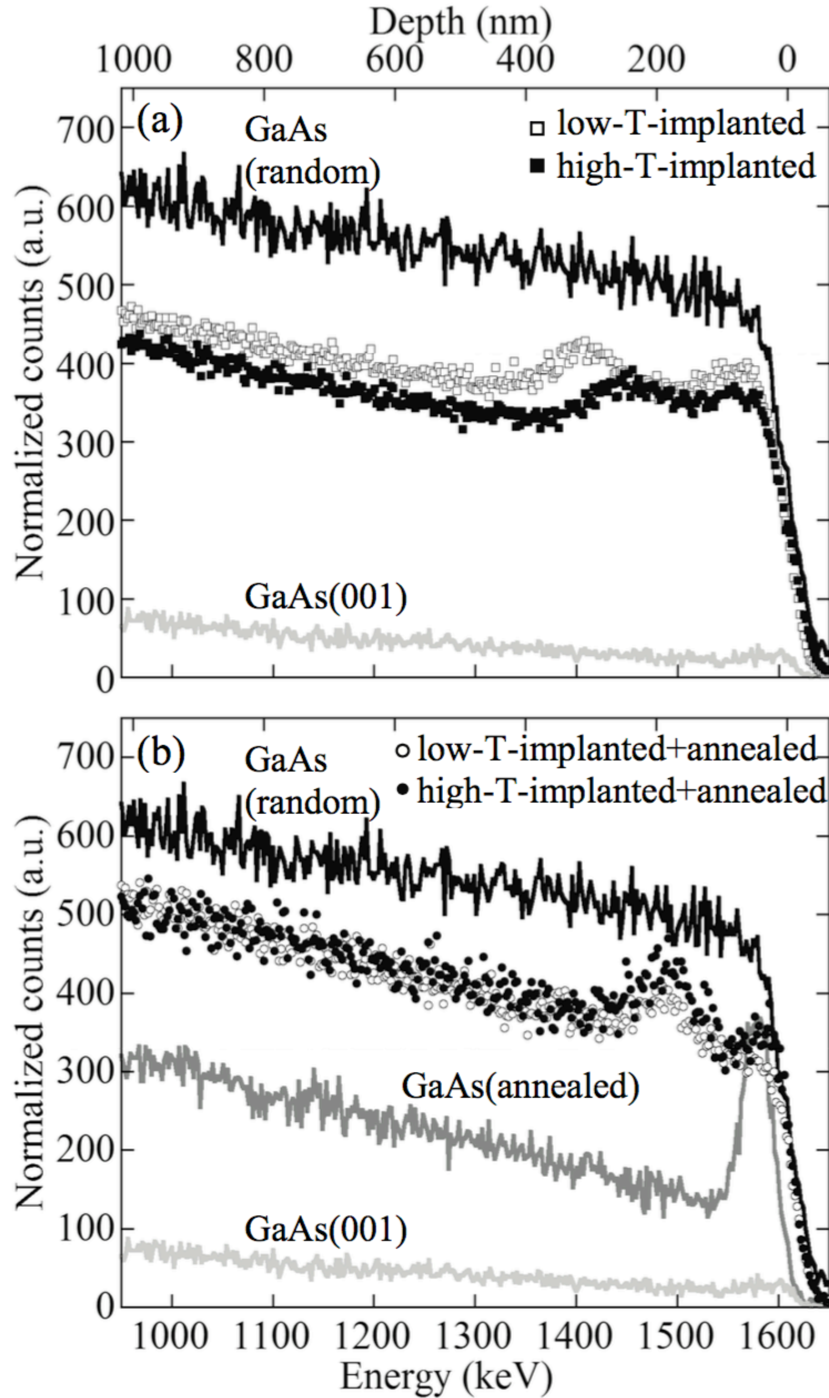

Fig. 4: Channeling-RBS spectra as a function of backscattered energy of GaAs layers (a) before and (b) after annealing, comparing low-*T*- (open symbols) and high-*T*- (closed symbols) implanted samples with GaAs in the random and (001) aligned configurations. In both cases, the normalized yield is similar for the low-*T* and high-*T* samples, suggesting similar lattice damage. The implanted-plus-annealed spectra in (b) exhibit local maxima at ~1480 keV (corresponding to ~200 nm) attributed to dechanneling by bubbles.